This is the accepted manuscript made available via CHORUS. The article has been published as:

Polarization Enhanced Deep Optical Dipole Trapping of math xmlns="http://www.w3.org/1998/Math/MathML" display="inline">mi mathvariant="normal">Λ/mi>/math>-Cooled Polar Molecules

Thomas K. Langin, Varun Jorapur, Yuqi Zhu, Qian Wang, and David DeMille

Phys. Rev. Lett. **127**, 163201 — Published 12 October 2021

DOI: 10.1103/PhysRevLett.127.163201

Polarization Enhanced Deep Optical Dipole Trapping of Λ-cooled Polar Molecules

Thomas K. Langin,[1,2] Varun Jorapur,[1,2] Yuqi Zhu,[1,2] Qian Wang,[1,2] and David DeMille[3]

[1] *Department of Physics, Yale University, New Haven, Connecticut, CT, 06520, USA*
[2] *Yale Quantum Institute, Yale University, New Haven, Connecticut 06520, USA*
[3] *Department of Physics, University of Chicago, Chicago, Illinois 60637, USA*

(Dated: August 12, 2021)

We demonstrate loading of SrF molecules into an optical dipole trap (ODT) via in-trap Λ-enhanced gray molasses cooling. We find that this cooling can be optimized by a proper choice of relative ODT and cooling beam polarizations. In this optimized configuration, we observe molecules with temperatures as low as $14(1)\,\mu$K in traps with depths up to 570 uK. With optimized parameters, we transfer $\sim$5% of molecules from our radio-frequency magneto-optical trap into the ODT, at a density of $\sim 2\times10^{9}\,\mathrm{cm}^{-3}$, a phase space density of $\sim 2\times10^{-7}$, and with a trap lifetime of $\sim$1 s.

Ultracold molecular gases can be produced by assembly from ultracold atoms [1–5], recently leading to the first demonstration of a quantum degenerate molecular gas [6], or by direct cooling and trapping of molecules. Recent progress on the latter path includes magneto-optical trapping (MOT) [7–10], sub-Doppler cooling [11, 12], loading into conservative magnetic quadrupole [13, 14] and optical dipole traps (ODTs) [15, 16], and observation of ultracold collisions [17–20]. These improvements bring us closer to realizing the potential utility of molecules for quantum simulation [21–24], quantum information [25, 26], and precision measurement [27–29].

These applications require gases with high density and low entropy, i.e., in or near the quantum degenerate regime. For directly cooled molecules, this will likely require collisional cooling [30–33], which requires achieving densities large enough for rapid collisional rethemalization. Increasing the initial phase-space density would minimize loss of molecules during collisional cooling.

In this Letter, we demonstrate the ability to reduce the temperature, T, (and thus maximize density, n, and phase space density, Φ) within an ODT of strontium monofluoride (SrF) by determining optimal polarizations of both the Λ-cooling (Fig. 1(b)) and trapping light. We have produced gases of up to $N_{ODT}\sim160$ molecules with $T\sim14\,\mu$K, $n\sim2\times10^{9}\,\mathrm{cm}^{-3}$, and $\Phi\sim2\times10^{-7}$ at trap depth $T_D\sim570\,\mu$K.

Our apparatus is illustrated in Fig. 1(a). SrF molecules from a cryogenic buffer gas beam source [34, 35] are slowed [36], then captured in an rfMOT [8, 37] ($N_{MOT}\sim$ 3500, $T_{MOT}\approx1$ mK, Gaussian width $\sigma_{MOT}\approx1$ mm). The rfMOT requires laser frequencies addressing all four $|X^2\Sigma^+, v=0, N=1, J, F\rangle$ hyperfine levels (Fig. 1(b)), coupling them to the $|A^2\Pi_{1/2}, v'=0, N'=0, J'=1/2, F'\rangle$ state, along with repumpers for the X($v=1,2,3$) vibrational states. To use laser power efficiently, a single beam containing all needed frequencies is cycled through all three orthogonal axes of the rfMOT, then retro-reflected, to provide trapping and cooling. To compensate for power loss along the path, an adjustable telescope is used to control the convergence of the MOT beams.

Efficiently loading an ODT typically requires $T\lesssim$

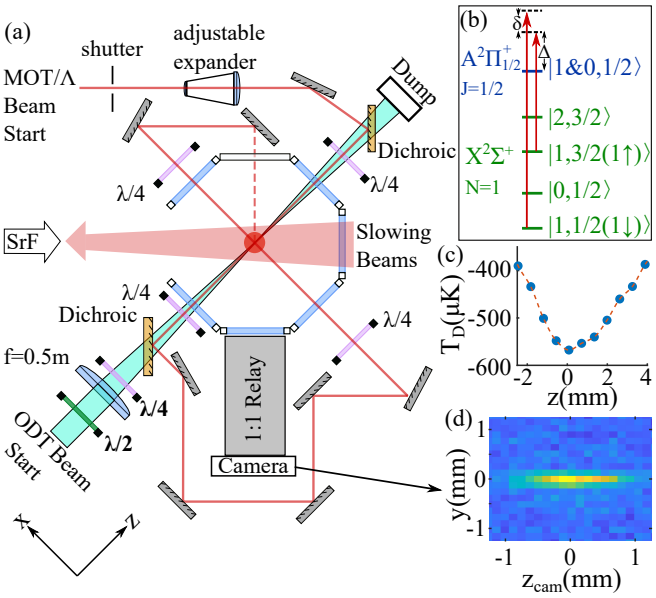

FIG. 1. (a) Experimental schematic. The MOT/Λ-cooling laser beams make three passes through the chamber before they are retroreflected (dashed line indicates the beam directed down below the chamber, then reflected upward). Additional waveplates (bottom left, bold labels) control the trap light polarization (see text). (b) Level diagram for Λ-cooling, with hyperfine sublevels $|F, J\rangle$ indicated. (c) Trap depth along ODT propagation axis (z) derived from measurements of the beam waist using a beam profiler. (d) *in-situ* image of optically trapped molecules.

$T_D/10$ [38]. Ideally, the cooling method should be effective both inside and outside the trap volume. One technique demonstrated to reach the required temperature in similar molecules (CaF and YO) requires coupling two $|X^2\Sigma, N=1\rangle$ hyperfine levels to $|A^2\Pi_{1/2}, J'=1/2\rangle$, with overall blue detuning Δ and relative Raman detuning δ (Fig. 1(b)), to create a Λ system [12, 15]. This 'Λ-cooling' approach combines gray molasses [11] with the velocity-selective coherent population trapping (VSCPT) characteristic of Λ systems [39, 40], and is commonly used for loading alkali atoms into ODTs [41]. In CaF, coupling the $|F=2\rangle$ and $|F=1\downarrow\rangle$ [throughout, $1\downarrow$ ($1\uparrow$)

refers to $|F=1, J=1/2(3/2)\rangle$] levels can cool molecules to $T\sim 10\,\mu$K in free space [15].

Although SrF has a very similar level structure to CaF, we find that coupling these states in SrF does *not* result in effective cooling. However, coupling $|1\uparrow\rangle$ and $|1\downarrow\rangle$ (Fig. 1(b)) does lead to $T \lesssim 10\,\mu$K for $\Delta \geq 2\pi\times 9\,\text{MHz}=1.4\Gamma$ (where $\Gamma = 2\pi\times 6.63\,\text{MHz}$ is the natural linewidth of the $X\rightarrow A$ transition). A numerical simulation based on solving the Optical Bloch Equations (OBEs) also shows that choosing $|1\uparrow\rangle$ over $|2\rangle$ to couple with $|1\downarrow\rangle$ results in stronger cooling in SrF [42].

In CaF, Λ-cooling was also shown to be effective within the ODT [15]. This is remarkable, since—unlike alkali atoms in their $|^2\text{S}_{1/2}\rangle$ ground state—molecules in a $|^2\Sigma, N=1\rangle$ state have substantial vector and tensor polarizabilities even for far-detuned traps [43], which lead to differential shifts between the substates of each hyperfine manifold that can destabilize the zero-velocity dark states needed for VSCPT cooling [44]. For example, Zeeman shifts of $\sim 100\,$kHz ($\sim 5\,\mu$K) can limit sub-Doppler cooling [11, 13, 44, 45]. The comparably large ODT-induced differential AC Stark shifts were proposed to explain the observed saturation of trapping efficiency of CaF at $T_D = 130\,\mu$K, since higher T_D leads to larger differential shifts [15].

We use Λ-cooling here to load SrF into an ODT. Unless otherwise indicated, $\Delta = 2\pi\times 22\,\text{MHz}$; $\delta = 2\pi\times 1.2\,\text{MHz}$; the total intensity from all 6 passes of the Λ laser beam, I, is $278\,\text{mW/cm}^2$; and the ratio of intensities coupling the hyperfine levels, $R_{1\uparrow,1\downarrow}$, is 2/3.

The ODT, formed by focusing a $\sim 50\,$W single-mode 1064 nm laser beam to a $1/e^2$-radius of $\sim 40\,\mu$m, is turned on simultaneously with the Λ-cooling. This laser is combined with one Λ-cooling beam pass using a dichroic mirror, then passes through a $\lambda/4$ plate before entering the chamber. Additional $\lambda/2$ and $\lambda/4$ waveplates (lower-left, Fig. 1(a)) are used to control the trap light polarization.

The trap depth is determined by calculating the AC Stark shift based on measured [46, 47] and/or calculated [48, 49] dipole matrix elements between $|X^2\Sigma\rangle$ and all other states [42]. By measuring the ODT beam profile along its axis (z), we determine the axial trap depth profile $T_D(z)$ (Fig. 1(c)), which deviates from ideal quadratic behavior due to astigmatism, and the trap frequencies, which are $\omega_{x,y,z} = 2\pi\times(1.7\times 10^3, 1.7\times 10^3, 9)\,\text{s}^{-1}$.

After 150 ms, the Λ-cooling light is shuttered for a time t_{sh} (50 ms unless noted), to allow untrapped molecules to fall from the imaging region. Then, Λ-cooling is turned back on for 150 ms, during which the camera is exposed. Trapped molecules remain cold even as they scatter photons [15], allowing for their fluorescence to be imaged *in situ* (Fig. 1(d)). This indicates that Λ-cooling is effective inside the trap. The peak ODT-induced scalar AC stark shift for the X state (A state) is -11.9 MHz (+0.4 MHz). These combine to redshift the one photon detuning in the trap center to $\Delta_{trap} = 2\pi\times 10\,\text{MHz}$, still blue enough to cool effectively.

Our imaging resolution is insufficient to observe the molecular cloud width along the short axes of the ODT, $\hat{x}$ and $\hat{y}$ (Fig. 1d). However, the weaker axial confinement makes the cloud density profile along the ODT axis, $n(z)$ (and associated width, σ_{ax}) resolvable by our camera, whose horizontal axis is at 45° to the ODT axis ($\hat{z}$). Then, T can be determined from $T_D(z)$ and $n(z)$. We also measured T through time-of-flight expansion and found results consistent with, albeit less precise than, those determined from $n(z)$.

We expected that in-trap cooling would be sensitive to the polarization of the trap laser, due to differential AC Stark shifts [43, 50–52] in the coupled manifolds (Fig. 2(f)). We anticipated that the optimum polarizations would be those for which two states, one within each manifold, experience the same shift (Fig. 2(f)) and thus form a coherent dark state both inside and outside the trap. Since there is no other applied field to define a quantization axis, we expected the cooling to depend only on the aspect ratio of the ODT light polarization ellipse [53], and not on its orientation or rotation direction.

Instead, we found that T can strongly depend on the rotation direction. To quantify this, we define the ellipticity, $\gamma_{ODT} = \frac{1}{2}\tan^{-1}\frac{S_3}{\sqrt{S_1^2+S_2^2}}$, where $S_{1,2,3}$ are the dimensionless Stokes parameters of the trap light [54]. The sign of γ_{ODT} indicates the electric field vector rotation direction, with $\gamma_{ODT}>0$ indicating clockwise (when viewing along the direction of light propagation); $\tan(\gamma_{ODT})$ is the ratio of minor to major axes of the polarization ellipse.

We found that the symmetry between positive and negative γ_{ODT} is broken by an intensity imbalance between the counter-propagating Λ-cooling beams, which have opposite circular polarizations. Such an imbalance can arise easily in our apparatus, where the Λ-cooling beam co-(counter)-propagating to the ODT beam is the last (first) pass of the long, retro-reflected, path (Fig. 1(a)). If the Λ-cooling beam is collimated, then, due to losses along the path, the ratio of intensities of final to first pass, $R_{I\Lambda}$, is 0.74. This can be increased (decreased) by making the beam mildly convergent (divergent).

The effect of this broken symmetry is shown in Fig. 2. Fig. 2(a) shows the results for $R_{I\Lambda} = 0.74$ when the Λ beam co-propagating with the ODT is σ^+ polarized. We find that σ_{ax}, and thus T, is minimized when the ODT polarization matches the weaker, co-propagating beam ($\gamma_{ODT} = +45°$). This remains the case when the Λ polarizations are reversed (Fig. 2(b)), where T is optimized when $\gamma_{ODT} = -45°$. If the intensity imbalance is reduced ($R_{I\Lambda} = 0.93$, Fig. 2(c)), the dependence on γ_{ODT} is much less pronounced (Fig. 2(d)). Ultimately, we find that T is globally minimized when the Λ beam intensities are deliberately imbalanced—in particular, when $R_{I\Lambda} = 0.74$

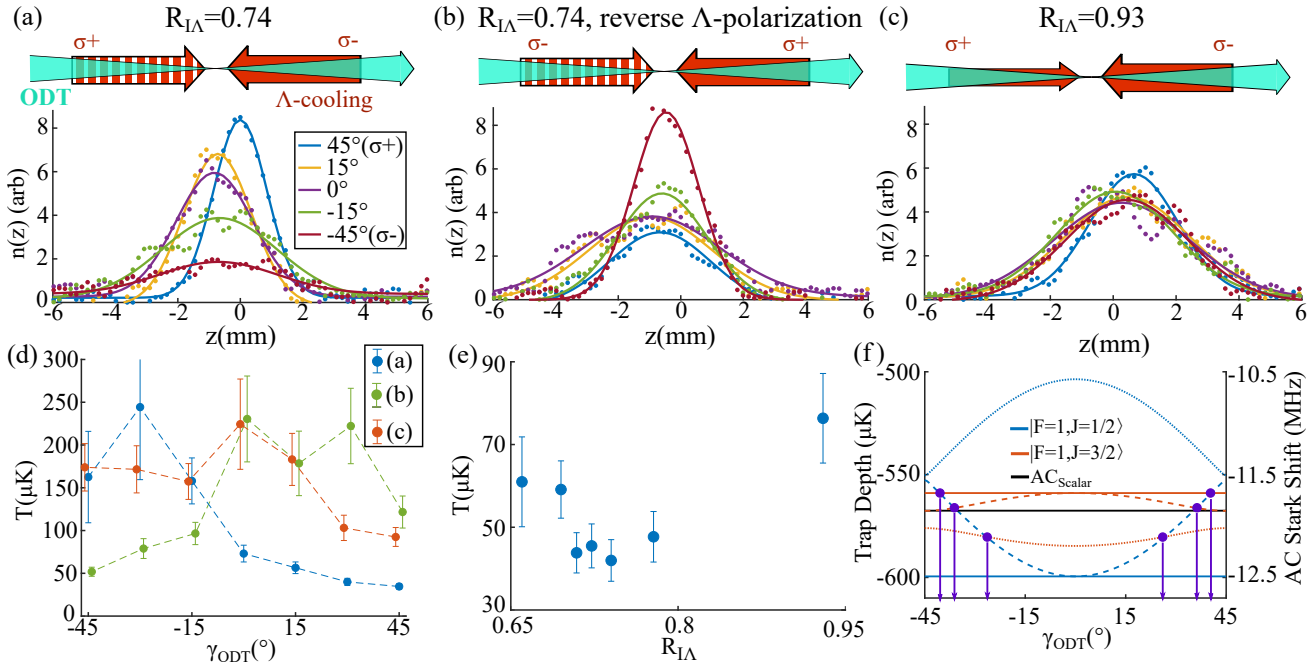

FIG. 2. (a)-(c) Trapped molecular cloud profiles for different $R_{I\Lambda}$ and γ_{ODT} (plot legends). (a-b) The trap is optimized when the ODT polarization matches that of the weaker of the two Λ beams (lower intensity indicated by red and white stripes) on its axis (see text). (c) If the imbalance is decreased such that $R_{I\Lambda} = 0.93$ (by making the beam convergent), the dependence on γ_{ODT} is reduced. (d) T, determined from fits to profiles in (a-c), vs. γ_{ODT}. (e) T vs $R_{I\Lambda}$ for $\gamma_{ODT} = +45°$, with Λ polarization as in (a). (f) Trap depth (and associated ODT-induced AC Stark Shift) for each eigenstate of the coupled manifolds vs. γ_{ODT} [42]. Purple circles indicate where a pair of states are degenerate.

and $\gamma_{ODT} = +45°$ (Fig. 2(e)) for the Λ polarizations in Fig. 2(a). This configuration is used throughout the rest of this paper. (As expected, we observe no dependence on the trap polarization ellipse orientation angle $\psi = \frac{1}{2}\tan^{-1}\frac{S_2}{S_1}$.)

To understand this unanticipated behavior, we developed an OBE solver [55] that can incorporate intensity imbalanced, retro-reflected beams. We explicitly add the AC Stark Hamiltonian from the ODT light (including vector and tensor shifts), while differential AC Stark shifts from the imbalanced Λ beams (which can be of comparable magnitude to those from the ODT laser under our conditions [42]) are included implicitly in the OBEs. This solver was benchmarked against results from comparable solvers [55, 56] and experimental observations, such as rfMOT trap temperature [8] and capture velocity, Λ-cooling [15], and single frequency cooling [45]. However, we were unable to reproduce the effects shown in Fig. 2. The mechanism behind the observed interplay between ODT polarization and Λ-beam intensity imbalance thus remains an open question.

We next worked to optimize δ and $R_{1\uparrow,1\downarrow}$. We observe that T is optimized near two-photon resonance ($\delta = 0$), with a broad minimum extending to $\delta > 0$ (Fig. 3a). Similar behavior has been observed in other experiments [15, 39, 57]. The breadth of this feature is comparable to the in-trap two photon Rabi frequency between

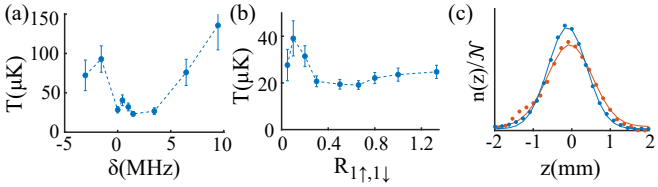

FIG. 3. Dependence of in-trap temperature, T, on Λ cooling parameters. (a) T vs δ, for $R_{1\uparrow,1\downarrow} = 2/3$. (b) T vs $R_{1\uparrow,1\downarrow}$ for $\delta = 2\pi \times 1.2\,\mathrm{MHz}$. (c) Examples of $n(z)/\mathcal{N}$, where $\mathcal{N} = \int n(z)dz$, with (blue, $T = 14\,\mu$K) and without (red, $T = 20\,\mu$K) fine spatial alignment of Λ-cooling beams.

the coupled hyperfine manifolds ($\Omega_\Lambda \approx 2\pi \times 7\,\mathrm{MHz}$ [42]), as expected. We also observe that T is optimized for $R_{1\uparrow,1\downarrow} \approx 2/3$ (Fig 3(b)). We note in particular that 'single frequency cooling' ($R_{1\uparrow,1\downarrow} = 0$)—which was shown to lead to $T < 10\,\mu$K in free space for CaF [45]—is ineffective at cooling SrF in the ODT, though it performed as well as optimized Λ-cooling in free space.

For optimal values of δ_R and $R_{1\uparrow,1\downarrow}$, we find that $T \sim 20\,\mu$K is regularly achievable. However, we have observed that T is sensitively dependent on the spatial alignment of the Λ-cooling beams. By iteratively adjusting the alignment while optimizing for T, we achieved a minimum of $T = 14(1)\,\mu$K (Fig. 3c). Because this optimal condition was difficult to maintain, the SrF cloud had

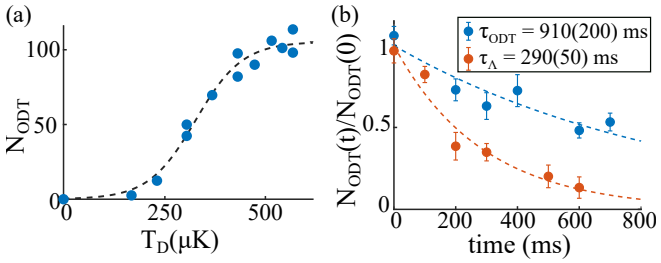

FIG. 4. (a) Number of molecules in ODT, N_{ODT}, vs trap depth, T_D, for optimum trap parameters [$\delta = 2\pi \times 1.2\,\mathrm{MHz}$, $\Delta = 2\pi \times 22\,\mathrm{MHz}$, $R_{1\uparrow,1\downarrow} = 2/3$]. For reference, typically $N_{MOT} \sim 3000$. The smooth curve is used to guide the eye. (b) Fraction of molecules remaining vs time with (red) and without (blue) Λ-cooling light. Dashed lines are exponential fits, with fit lifetime indicated in the legend.

the more typical temperature in the data shown throughout this paper.

Next, we studied the dependence of number of trapped molecules, N_{ODT}, on trap depth (Fig. 4(a)). Knowing this dependence is necessary to optimize the transverse trap shape for maximum N_{ODT}. For this measurement, we recapture the molecules in an rfMOT prior to imaging. This is done by turning on the rfMOT coils and switching from the Λ-cooling laser configuration to the rfMOT configuration. After the ODT is loaded, but prior to recapture, we turn off all cooling light for $t_{sh} = 140\,\mathrm{ms}$ to ensure that untrapped molecules fall out of the rfMOT capture volume.

We find that N_{ODT} rises monotonically with trap depth, but appears to saturate for $T_D \gtrsim 500\,\mu\mathrm{K}$. This is strikingly different than was observed in ODT loading of CaF, where the efficiency peaked at $T_D \sim 130\,\mu\mathrm{K}$ [15]. We suspect that this difference relates to the states chosen for Λ-cooling. Hyperfine induced mixing between $|1\downarrow\rangle$ and $|1\uparrow\rangle$ modifies the transition strengths from the $|A\Pi_{1/2}, J' = 1/2, F'\rangle$ hyperfine states to these levels. In SrF, $|1\uparrow\rangle$ couples 56× more strongly to $|F' = 0\rangle$ than to $|F' = 1\rangle$ [42], so we expect that the Λ system primarily couples through the former, thus avoiding complications that may arise due to the large vector light shift in the latter [42]. If the $|2\rangle$ and $|1\downarrow\rangle$ states are used, as in CaF [15], the coupling must be through $|F' = 1\rangle$. The larger number of sublevels, all of which experience differential shifts, in the latter scheme may also limit Λ-cooling in deeper ODTs.

Another critical trap quantity is the lifetime τ_{ODT}. To study collisions, it is necessary to have $\tau_{ODT}^{-1} \lesssim \beta n$, where β is the collisional rate coefficient. We measure τ_{ODT} by shuttering the Λ-cooling light for a variable time before re-opening the shutter and imaging the remaining molecules. We find $\tau_{ODT} = 910(200)\,\mathrm{ms}$ (Fig. 4(b)). Since this is comparable to the lifetime we measure in a magnetic quadrupole trap with the same background pressure [13], we believe the lifetime in both cases is limited by collisions with background gas.

We also measure the trap lifetime while Λ-cooling is applied, τ_Λ. This quantity sets the time over which molecule loading is effective and over which *in-situ* imaging can occur. To measure τ_Λ, we continuously apply the Λ light for an additional $t_c = 650\,\mathrm{ms}$ after the 150 ms loading and 50 ms release times, and image for 50 ms intervals during t_c.

We measure $\tau_\Lambda = 290(50)\,\mathrm{ms}$, similar to what was observed in an ODT of CaF [15]. There, the losses were attributed to spatial diffusion out of the trap induced by light scattering. However, Monte Carlo simulations indicate that this should contribute negligibly to the SrF loss rate, primarily due to the larger trap depths used here in addition to the higher mass of SrF. Light-assisted collisions represent another potential loss mechanism. Λ-light assisted loss rate coefficients of $\beta \gtrsim 10^{-9}\,\mathrm{cm}^3/\mathrm{s}$ have been observed in diatomic molecules held in optical tweezers [19], and thus could limit lifetimes to the few 100 ms level at our typical peak density of $10^9\,\mathrm{cm}^{-3}$.

For applications where high-fidelity detection is critical, such as studying molecules trapped in optical tweezers [17, 19], it is important for the average number of photons emitted per molecule before loss ($\tau_\Lambda R_\Lambda$, where R_Λ is the scattering rate during Λ-cooling) to be large. We measure $R_\Lambda = 3.1 \times 10^5\,\mathrm{s}^{-1}$ by comparing the fluorescence collected with that from the MOT recapture, where the scattering rate is known [8]. Thus, $\tau_\Lambda R_\Lambda = 9(2) \times 10^4$, ∼3 times larger than demonstrated in an ODT of CaF [15] despite the similar t_Λ. We attribute the larger R_Λ observed here to the smaller in-trap detuning ($\Delta_{trap}/\Gamma = 1.5$ here, compared to $\Delta_{trap}/\Gamma = 3.6$ in [15]).

In conclusion, by optimizing the combination of trap light polarization and intensity imbalance of Λ-cooling lasers, we have loaded ∼ 5% of SrF molecules from an rfMOT into a 570 μK deep ODT, at temperatures as low as 14(1) μK. The large value of T_D/T implies strong compression, yielding density and phase space density higher than previously reported in bulk gases of directly cooled molecules, despite starting with 10 times fewer molecules.

We find that several features of loading molecule ODTs using Λ-cooling remain poorly understood, such as the observed interplay between the trap polarization and cooling light intensity imbalance, and, more generally, the effect of vector and tensor light shifts. Once these are better understood, higher trap compression may be achievable.

We are working to increase both the number of molecules in our rfMOT and the ODT loading efficiency. If collisional loss is described by the universal loss rate coefficient β_0 [58], then, for the compression achieved here, a factor of 5 increase in N_{ODT} would lead to a collisional timescale $\tau_0 = (\beta_0 n)^{-1} \sim \tau_{ODT}$, allowing for the first studies of ultracold SrF molecule collisions.

We gratefully acknowledge support from AFOSR,

ONR, ARO (DURIP), and the Yale Quantum Institute. We thank Loic Anderegg for helpful discussions.

[1] K. K. Ni, S. Ospelkaus, M. H. G. de Miranda, A. Pe'er, B. Neyenhuis, J. J. Zirbel, S. Kotochigova, P. S. Julienne, D. S. Jin, and J. Ye, A high phase-space-density gas of polar molecules, Science **322**, 231 (2008).

[2] P. K. Molony, P. D. Gregory, Z. Ji, B. Lu, M. P. Koppinger, C. R. L. LeSueur, C. L. Blackley, J. M. Hutson, and S. L. Cornish, Creation of ultracold $^{87}Rb^{133}Cs$ molecules in the rovibrational ground state, Phys. Rev. Lett. **113**, 255301 (2014).

[3] J. W. Park, S. A. Will, and M. W. Zwierlein, Ultracold dipolar gas of fermionic $^{23}Na^{40}K$ molecules in their absolute ground state, Phys. Rev. Lett. **114**, 205302 (2015).

[4] M. Guo, B. Zhu, B. Lu, X. Ye, F. Wang, R. Vexiau, N. Bouloufa-Maafa, G. Quemener, O. Dulieu, and D. Wang, Creation of an ultracold gas of ground-state dipolar $^{23}Na^{87}Rb$ molecules, Phys. Rev. Lett. **116**, 205303 (2016).

[5] T. M. Rvachov, H. Son, A. T. Sommer, S. Ebadi, J. J. Park, M. W. Zwierlein, W. Ketterle, and A. O. Jamison, Long-lived ultracold molecules with electric and magnetic dipole moments, Phys. Rev. Lett. **119**, 143001 (2017).

[6] L. D. Marco, G. Valtolina, K. Matsuda, W. G. Tobias, J. P. Covey, and J. Ye, A degenerate fermi gas of polar molecules, Science **363**, 853 (2019).

[7] J. F. Barry, D. J. McCarron, E. B. Norrgard, M. H. Steinecker, and D. DeMille, Magneto-optical trapping of a diatomic molecule, Nature **512**, 286 (2014).

[8] E. B. Norrgard, D. J. McCarron, M. H. Steinecker, M. R. Tarbutt, and D. DeMille, Submillikelvin dipolar molecules in a radio-frequency magneto-optical trap, Phys. Rev. Lett. **116**, 063004 (2016).

[9] L. Anderegg, B. L. Augenbraun, E. Chae, B. Hemmerling, N. R. Hutzler, A. Ravi, A. Collopy, J. Ye, W. Ketterle, and J. M. Doyle, Radio frequency magneto-optical trapping of CaF with high density, Phys. Rev. Lett. **119**, 103201 (2017).

[10] A. L. Collopy, S. Ding, Y. Wu, I. A. Finneran, L. Anderegg, B. L. Augenbraun, J. M. Doyle, and J. Ye, 3D magneto-optical trap of yttrium monoxide, Phys. Rev. Lett. **121**, 213201 (2018).

[11] S. Truppe, H. J. Williams, M. Hambach, L. Caldwell, N. J. Fitch, E. A. Hinds, B. E. Sauer, and M. R. Tarbutt, Molecules cooled below the doppler limit, Nature Phys. **13**, 1173 (2017).

[12] S. Ding, Y. Wu, I. A. Finneran, J. J. Burau, and J. Ye, Sub-doppler cooling and compressed trapping of YO molecules at μK temperatures, Phys. Rev. X. **10**, 021049 (2020).

[13] D. J. McCarron, M. H. Steinecker, Y. Zhu, and D. DeMille, Magnetic trapping of an ultracold gas of polar molecules, Phys. Rev. Lett. **121**, 013202 (2018).

[14] H. J. Williams, L. Caldwell, N. J. Fitch, S. Truppe, J. Rodewald, E. A. Hinds, B. E. Sauer, and M. R. Tarbutt, Magnetic trapping and coherent control of laser-cooled molecules, Phys. Rev. Lett. **120**, 163201 (2018).

[15] L. W. Cheuk, L. Anderegg, B. L. Augenbraun, Y. Bao, S. Burchesky, W. Ketterle, and J. M. Doyle, Λ-enhanced imaging of molecules in an optical trap, Phys. Rev. Lett. **121**, 083201 (2018).

[16] L. Anderegg, B. L. Augenbraun, Y. Bao, S. Burchesky, L. W. Cheuk, W. Ketterle, and J. M. Doyle, Laser cooling of optically trapped molecules, Nature Phys. **14**, 890 (2018).

[17] L. W. Cheuk, L. Anderegg, Y. Bao, S. Burchesky, S. S. Yu, W. Ketterle, K. K. Ni, and J. M. Doyle, Observation of collisions between two ultracold ground-state CaF molecules, Phys. Rev. Lett. **125**, 043401 (2020).

[18] L. Anderegg, S. Burchesky, Y. Bao, S. Yu, T. Karman, E. Chae, K. K. Ni, W. Ketterle, and J. M. Doyle, Observation of microwave shielding of ultracold molecules, arXiv:2102.04365.

[19] L. Anderegg, L. W. Cheuk, Y. Bao, S. Burchesky, W. Ketterle, K. K. Ni, and J. M. Doyle, An optical tweezer array of ultracold molecules, Science **365**, 1156 (2019).

[20] S. Jurgilas, A. Chakraborty, C. J. H. Rich, L. Caldwell, H. J. Williams, N. J. Fitch, B. E. Sauer, M. D. Frye, J. M. Hutson, and M. R. Tarbutt, Collisions between ultracold molecules and atoms in a magnetic trap, Phys. Rev. Lett. **126**, 153401 (2021).

[21] L. D. Carr, D. DeMille, R. V. Krems, and J. Ye, Cold and ultracold molecules: science, technology and applications, New J. Phys. **11**, 055049 (2009).

[22] A. Micheli, G. K. Brennen, and P. Zoller, A toolbox for lattice-spin models with polar molecules, Nature Phys. **2**, 341 (2006).

[23] G. Pupillo, A. Griessner, A. Micheli, M. Ortner, D. W. Wang, and P. Zoller, Cold atoms and molecules in self-assembled dipolar lattices, Phys. Rev. Lett. **100**, 050402 (2008).

[24] H. P. Buchler, E. Demler, M. Lukin, A. Micheli, N. Prokofev, G. Pupillo, and P. Zoller, Strongly correlated 2d quantum phases with cold polar molecules: Controlling the shape of the interaction potential, Phys. Rev. Lett. **98**, 060404 (2007).

[25] D. DeMille, Quantum computation with trapped polar molecules, Phys. Rev. Lett. **88**, 067901 (2002).

[26] S. F. Yelin, K. Kirby, and R. Cote, Schemes for robust quantum computation with polar molecules, Phys. Rev. A. **74**, 050301(R) (2006).

[27] J. Lim, J. R. Almond, M. A. Trigatzis, J. A. Devlin, N. J. Fitch, B. E. Sauer, M. R. Tarbutt, and E. A. Hinds, Laser cooled YbF molecules for measuring the electrons electric dipole moment, Phys. Rev. Lett. **120**, 123201 (2018).

[28] ACME Collaboration, Improved limit on the electric dipole moment of the electron, Nature **562**, 355 (2018).

[29] W. B. Cairncross, D. N. Gresh, M. Grau, K. C. Cossel, T. S. Roussy, Y. Ni, Y. Zhou, J. Ye, and E. A. Cornell, Precision measurement of the electrons electric dipole moment using trapped molecular ions, Phys. Rev. Lett. **119**, 153001 (2017).

[30] C. J. Myatt, E. A. Burt, R. W. Ghrist, E. A. Cornell, and C. E. Wieman, Production of two overlapping bose-einstein condensates by sympathetic cooling, Phys. Rev. Lett. **78**, 586 (1997).

[31] I. Bloch, M. Greiner, O. Mandel, T. W. Hansch, and T. Esslinger, Sympathetic cooling of ^{85}Rb and ^{87}Rb, Phys. Rev. A. **64**, 021402(R) (2001).

[32] H. Son, J. J. Park, W. Ketterle, and A. O. Jamison, Collisional cooling of ultracold molecules, Nature **580**, 197 (2020).

[33] G. Valtolina, K. Matsuda, W. Tobias, J. R. Li, L. D. Marco, and J. Ye, Dipolar evaporation of reactive molecules to below the fermi temperature, Nature **588**, 239 (2020).

[34] J. F. Barry, E. S. Shuman, and D. DeMille, A bright, slow cryogenic molecular beam source for free radicals, Phys. Chem. Chem. Phys. **13**, 18936 (2011).

[35] N. R. Hutzler, H. Lu, and J. M. Doyle, The buffer gas beam: An intense, cold, and slow source for atoms and molecules, Chem. Rev. **112**, 4803 (2012).

[36] J. F. Barry, E. S. Shuman, E. B. Norrgard, and D. DeMille, Laser radiation pressure slowing of a molecular beam, Phys. Rev. Lett. **108**, 103002 (2012).

[37] M. H. Steinecker, D. J. McCarron, Y. Zhu, and D. DeMille, Improved radiofrequency magnetooptical trap of srf molecules, ChemPhysChem **17**, 3664 (2016).

[38] K. M. O'Hara, S. R. Granade, M. E. Gehm, and J. E. Thomas, Loading dynamics of CO_2 laser traps, Phys. Rev. A. **63**, 043403 (2001).

[39] A. T. Grier, I. Ferrier-Barbut, B. S. Rem, M. Delehaye, L. Khaykovich, F. Chevy, and C. Salomon, Λ-enhanced sub-doppler cooling of lithium atoms in D1 gray molasses, Phys. Rev. A. **87**, 063411 (2013).

[40] A. Aspect, E. Arimondo, R. Kaiser, N. Vansteenkiste, and C. Cohen-Tannoudji, Laser cooling below the one-photon recoil energy by velocity-selective coherent population trapping, Phys. Rev. Lett. **61**, 826 (1988).

[41] A. Burchianti, G. Valtolina, J. A. Seman, E. Pace, M. De-Pas, M. Inguscio, M. Zaccanti, and G. Roati, Efficient all-optical production of large ^{6}Li quantum gases using D1 gray-molasses cooling, Phys. Rev. A. **90**, 043408 (2014).

[42] See supplemental material at [url will be inserted by publisher] for information on ac stark matrix calculations and two photon rabi frequency calculations, .

[43] S. Kotochigova and D. DeMille, Electric-field-dependent dynamic polarizability and state-insensitive conditions for optical trapping of diatomic polar molecules, Phys. Rev. A. **82**, 063421 (2010).

[44] D. Boiron, C. Triche, D. R. Meacher, P. Verkerk, and G. Grynberg, Three-dimensional cooling of cesium atoms in four-beam gray optical molasses, Phys. Rev. A. **52**, R3425 (1995).

[45] L. Caldwell, J. A. Devlin, H. J. Williams, N. J. Fitch, E. A. Hinds, B. E. Sauer, and M. R. Tarbutt, Deep laser cooling and efficient magnetic compression of molecules, Phys. Rev. Lett. **123**, 033202 (2019).

[46] P. J. Dagdigian, H. W. Cruse, and R. N. Zare, Radiative lifetimes of the alkaline earth monohalides, J. Chem. Phys. **60**, 2330 (1974).

[47] L. E. Berg, K. Ekvall, T. Hansson, A. Iwamae, V. Zengin, D. Husain, and P. Royen, Time-resolved measurements of the $B^2\Sigma$ state of SrF by laser spectroscopy, Chemical Physics Letters **248**, 283 (1996).

[48] NL-eEDM Collaboration, High accuracy theoretical investigations of CaF, SrF, and BaF and implications for laser-cooling, J. Chem. Phys. **151**, 034302 (2019).

[49] G. Fernando de Melo and F. R. Ornellas, The Λ+S and Ω electronic states of srf below 40,000 cm^{-1}: A theoretical contribution, Journal of Quantitative Spectroscopy & Radiative Transfer **237**, 106632 (2019).

[50] B. Neyenhuis, B. Yan, S. A. Moses, J. P. Covey, A. Chotia, A. Petrov, S. Kotochigova, J. Ye, and D. S. Jin, Anisotropic polarizability of ultracold polar $^{40}K^{87}Rb$ molecules, Phys. Rev. Lett. **109**, 230403 (2012).

[51] P. D. Gregory, J. A. Blackmore, J. Aldegunde, J. M. Hutson, and S. L. Cornish, ac stark effect in ultracold polar $^{87}Rb^{133}Cs$ molecules, Phys. Rev. A. **96**, 021402(R) (2017).

[52] J. Lin, J. He, X. Ye, and D. Wang, Anisotropic polarizability of ultracold ground-state $^{23}Na^{87}Rb$ molecules, Phys. Rev. A. **103**, 023332 (2021).

[53] T. Rosenbrand, D. D. Grimes, and K. K. Ni, Elliptical polarization for molecular stark shift compensation in deep optical traps, Opt. Express **26**, 19821 (2018).

[54] E. Hecht, *Optics* (Pearson Education Limited, Harlow, Essex, United Kingdom, 2017).

[55] J. A. Devlin and M. R. Tarbutt, Laser cooling and magneto-optical trapping of molecules analyzed using optical bloch equations and the fokker-planck-kramers equation, Phys. Rev. A. **98**, 063415 (2018).

[56] J. A. Devlin and M. R. Tarbutt, Three-dimensional doppler, polarization-gradient, and magneto-optical forces for atoms and molecules with dark states, New J. Phys. **18**, 123017 (2016).

[57] S. Rosi, A. Burchianti, S. Conclave, D. S. Naik, G. Roati, C. Fort, and F. Minardi, Λ-enhanced grey molasses on the D2 transition of rubidium-87 atoms, Scientific Reports **8**, 1301 (2018).

[58] Z. Idziaszek and P. S. Julienne, Universal rate constants for reactive collisions of ultracold molecules, Phys. Rev. Lett. **104**, 113202 (2010).

[59] P. M. Sheridan, J. Wang, M. J. Dick, and P. F. Bernath, Optical-optical double resonance spectroscopy of the $C^2\Pi$-$A^2\Pi$ and $D^2\Sigma^+$-$A^2\Pi$ transitions of SrF, J. Phys. Chem. A **113**, 13383 (2009).

[60] W. E. Ernst and J. O. Schroder, The $B^2\Sigma^+$-$X^2\Sigma^+$ system of SrF: Precise spectroscopic constants from a combined fit of microwave and sub-doppler optical spectra, Chemical Physics **78**, 363 (1983).

[61] P. M. Sheridan, J. Wang, M. J. Dick, and P. F. Bernath, Optical-optical double resonance spectroscopy of SrF: The $F^2\Sigma^+$-$B^2\Sigma^+$ and $G^2\Pi$-$B^2\Sigma^+$ systems, Chem. Phys. Lett. **148**, 130 (1988).

[62] J. K.G. Watson, Honl-london factors for multiplet transitions in hund's case a or b, Journal of Molecular Spectroscopy **252**, 5 (2008).

[63] T. E. Wall, J. F. Kanem, J. J. Hudson, B. E. Sauer, D. Cho, M. G. Boshier, E. A. Hinds, and M. R. Tarbutt, Lifetime of the $A(v' = 0)$ state and Franck-Condon factor of the $A - X(0 - 0)$ transition of CaF measured by the saturation of laser-induced fluorescence, Phys. Rev. A. **78**, 062509 (2008).

[64] J. R. P. Angel and P. G. H. Sanders, The hyperfine structure stark effect i. theory, Proceedings of the Royal Society of London, Series A., Mathematical and Physical Sciences **305**, 125 (1968).